Flexible and Printed Electronics

PAPER

Screen printable PANI/carbide-derived carbon supercapacitor electrode ink with chitosan binder

Ezgi Inci Yesilyurt[1,2], Jürgen Pionteck[1], Jari Keskinen[3], Aapo Kattainen[3], Timo Punkari[3], Frank Simon[1], Matti Mäntysalo[3] and Brigitte Voit[1,2,*]

[1] Leibniz Institute of Polymer Research Dresden, Dresden, Germany
[2] Faculty of Chemistry and Food Chemistry, Technische Universität Dresden, 01062 Dresden, Germany
[3] Faculty of Information Technology and Communication Sciences, Tampere University, Tampere, Finland
* Author to whom any correspondence should be addressed.

E-mail: voit@ipfdd.de

Keywords: carbide-derived carbon, chitosan, polyaniline, printed electronics, screen printing, supercapacitor

Supplementary material for this article is available online

OPEN ACCESS

RECEIVED
1 September 2023

REVISED
30 October 2023

ACCEPTED FOR PUBLICATION
21 November 2023

PUBLISHED
7 December 2023

Abstract

Polyaniline (PANI)/carbide-derived carbon (CDC) was synthesized by using *in-situ* chemical oxidative polymerization of PANI in presence of CDC. Conductive electrode ink materials were prepared by using eco-friendly chitosan binder in water media. In the following, symmetrical supercapacitors (SCs) were fabricated by both doctor blade coating and screen printing technique. The electrical conductivity, morphology, specific capacitance, and energy density of these composites were evaluated for their applicability as SC electrodes. Pure PANI with chitosan binder was not printable because of its brittleness, however, the presence of CDC allows the preparation of smooth films which are suitable for electrode preparation. The fabricated composite electrode has a higher specific capacitance (up to 419 F g^{-1}) and higher energy density (up to 6.7 W h kg^{-1}) compared to the pristine CDC electrode. The capacitance of screen-printed SCs was 440–470 mF with an equivalent series resistance of about 27 Ω.

1. Introduction

Supercapacitors (SCs), also known as electrochemical capacitors, have excellent power performance, strong reversibility, a long cycle life, a simple operating mode and are easy to integrate with electronic devices [1, 2]. SCs are typically classified into two distinct categories based on their energy storage mechanism: electrical double layer capacitors (EDLCs) and pseudocapacitors. The mechanism of EDLCs derives capacitance from the simple accumulation of electrostatic charge at the electrode/electrolyte interface. Therefore, materials with high surface area that is accessible to the electrolyte ions need to be used. In the particular case of pseudocapacitors, Faradaic processes take place due to fast and reversible electroactive species [3–5].

Metal oxides, metal-doped carbons and conducting polymers have shown pseudocapacitance behavior which is based on Faradaic redox reactions [6]. Such electrode materials enable the development of SCs with higher energy density. Polyacetylenes, polyanilines, polypyrroles and polythiophenes, are known to be among the most common conducting polymers [7, 8]. Among these polymers, polyaniline, an intrinsically conductive polymer with pseudocapacitive performance, has been widely used as an electroactive material. Polyaniline (PANI) is electrically conductive, low cost and offers a wide range of morphologies [9, 10]. However, owing to ion insertion and removal, electrodes are unstable at high scan rates and during long cycling [11]. In addition, it has low mechanical resistance and is unable to create a durable film on the different current collectors. Besides, the production of uniform printed electrode materials using PANI on larger scales for energy storage applications poses significant challenges. To address these particular challenges, researchers have investigated hybrid structures that contain compositions of PANI and carbon [12, 13]. The inclusion of carbon structures in these compositions offers several advantages, including enhanced electrical conductivity, increased surface area, and improved mechanical and chemical strength, which helps in overcoming the

previously mentioned issue [14, 15]. Activated carbons (ACs) [16, 17], carbon aerogels [18], carbon nanotubes (CNTs) [19], graphene [20], and carbide-derived carbons (CDCs) [21] can be used as a carbon electrode materials. Metal carbides like SiC, TiC, NbC, Al_4C_3, Ti_3SiC_2, etc can be converted into bulk and powdered CDCs by elevated temperature processes. It is possible to optimize CDCs with high specific surface area by adjusting the initial carbide and treatment temperature to provide a promising electrode active material for SCs [22, 23].

Poly(vinylidene fluoride) [24], poly(vinyl alcohol) [25], poly(vinylpyrrolidone) [26], Nafion [27], cellulose including carboxymethyl cellulose [28], and chitosan are some of the used traditional binders. The efficiency of the SC electrode is greatly affected by the binders used. Each of them has its own unique features, such as flexibility, non-toxicity, chemical inertness, good adhesion, and solubility [29]. Among these binders, chitosan is commonly utilized in battery systems thanks to its appropriate characteristics [30]. It has high thermal stability, maintaining stable at temperatures up to 200 °C [31]. Previous research demonstrated that the composite film of chitosan/graphene had higher tensile strengths than pure chitosan film, demonstrating that the chitosan binder can provide sufficient mechanical strength to bind the graphene [32]. Moreover, chitosan solution with acetic acid can be used to make water-based AC inks for printable SC electrodes [33].

Aqueous electrolytes, organic electrolytes, and ionic liquids are types of electrolytes used in SCs. When choosing proper electrolyte, it is essential to consider factors like voltage range, specific capacitance, equivalent series resistance (ESR), power density, corrosion resistance, and toxicity [34]. The key benefits of aqueous electrolytes are their low price, and high electrical conductivity. Additionally, neutral electrolytes may provide a wider potential window than acidic or alkaline electrolytes; hence, SCs that consist of neutral electrolytes are capable of achieving a higher energy density [35, 36]. Previous research established the possibility of 0.5 M Na_2SO_4 solution as a neutral electrolyte for PANI electrodes in SC applications [37, 38].

With printing technologies, SCs can be manufactured with many benefits, including precise control over their geometric shape, thickness, composition, and physical properties, low costs, minimal environmental impact, and high compatibility with substrates. The performance of screen-printed SCs is significantly dependent on the ink utilized during the printing process [39, 40]. It is essential to conduct research on the optimal materials for formulating efficient inks. Previous studies have shown that conductive polyaniline carbon composite ink patterns can be produced by screen printing for various applications.

Several related studies on AC, CNTs, and graphene coated with PANI have been reported so far, however there are fewer publications on the *in-situ* production of PANI/CDC composite by chemical oxidative polymerization [41]. In this study, PANI/CDC hybrid composites are fabricated by using *in situ* chemical oxidative polymerization with various monomer to carbon ratios. From these composites, printable water-based ink materials were prepared by using environmentally friendly chitosan as a binder. As far as we know, the utilization of an eco-friendly and water-based chitosan binder for the fabrication of this particular kind of electrode material and its printability has not been previously reported. The results demonstrated that the inclusion of CDC enhances the processability of inks containing PANI, enabling the fabrication of electrodes by doctor blade and screen-printing techniques. In this study, the electrochemical performance of these electrodes is discussed in detail.

2. Experimental

2.1. Materials

Aniline (99.8%, Acros Organics, Belgium), hydrochloric acid (HCl, 37%, Merck, Germany), and ammonium persulfate (APS, 98%, Sigma Aldrich, Darmstadt, Germany) were selected for synthesis of polyaniline. CDC (CDC, Skeleton Technologies) was selected for the preparation of high surface carbon structures and synthesis of PANI/CDC composites.

Sodium sulfate (Na_2SO_4, Sigma Aldrich, USA, 99.0 wt%), and the thin graphite sheet current collector T68A (T-Global Technology Co., Ltd, UK, thicknesses of the layers 35 μm with adhesive), graphite ink (Acheson ELECTRODAG PF-407C), DuPont™ Kapton® 200HN film (50 μm thickness, KREMPEL GmbH, Germany), were used for the preparation of electrolytes and current collectors, respectively. Chitosan (shrimp shells low-viscous, Sigma-Aldrich, Germany) was used as a non-toxic binder.

2.2. Synthesis of PANI

PANI was synthesized by chemical oxidative polymerization. APS was chosen as an oxidant [42]. 150 ml 1 M HCl solution was filled into a round bottomed flask. Aniline (1 g, 10.7 mmol) was added under rigorous stirring (ice bath (0 °C–4 °C), 4 h, 250 rpm). APS (2.45 g, 10.7 mmol) dissolved in 50 ml of 1 M HCl solution was then added dropwise to the reaction medium. The reaction was performed at 0 °C–4 °C for approximately 4 h and then continued 24 h at 20 °C. The product was filtered and washed with 1 l Millipore water, 0.5 l ethanol and 0.5 l acetone. Finally, the obtained powder was dried in a vacuum oven at 100 °C for 24 h.

2.3. Synthesis of PANI/CDC composites

The PANI/CDC composites were synthesized using a similar method as described in our previous work on

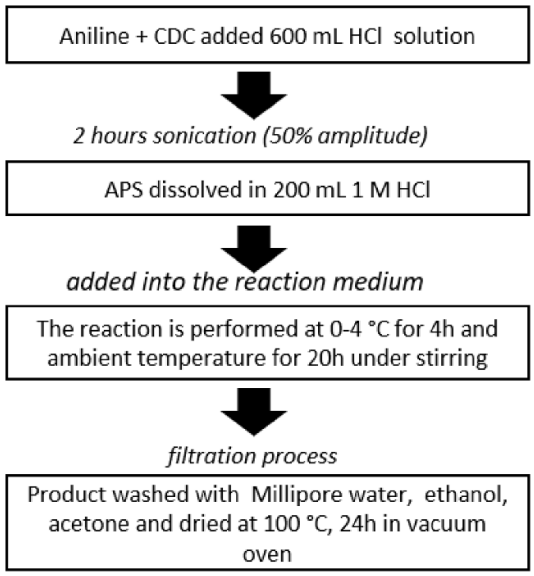

Figure 1. Diagram of the synthesis process of PANI/CDC composites.

Table 1. Synthesis compositions and yields of PANI/CDC composites.

Sample	Aniline: APS (molar ratio)	Mass (Aniline) (g)	Mass (CDC) (g)
PANI/CDC (5:1)	1:1	20	4
PANI/CDC (10:1)	1:1	20	2
PANI/CDC (30:1)	1:1	20	0.66

PANI/MWCNT composites [43]. Diagram of the synthesis process of PANI/CDC composites is shown in figure 1.

According to the composition, the composites are labelled PANI/CDC (mass ratio of aniline: CDC). These are, respectively, PANI/CDC (5:1), PANI/CDC (10-1) and PANI/CDC (30-1). For each composite, the yield of the final powder product is roughly 20 g (table 1).

2.4. Preparation of electrode inks with chitosan binder

The electrode inks were manufactured by utilizing a non-toxic chitosan binder, following the methodology outlined in our previous research [43]. In its dried state, ink is composed of approximately 5.4% binder and 94.6% active material (by mass).

For screen printing, the viscosity of the prepared PANI/CDC ink was measured with Anton Paar MCR 301 rheometer. Parallel plate geometry was used with 1 mm gap and measurement was performed between a shear rate of 0.01–100 s^{-1}.

2.5. Fabrication of symmetrical SCs by doctor blade method

Fabricated symmetrical SCs are used in two electrode measurements. The fabrication of SCs was carried out on poly (ethylene terephthalate) (PET) film, specifically Melinex ST506 from DuPont Teijin Films, with a thickness of 125 μm. Ultraviolet-ozone plasma treatment was applied to the current collectors for 60 min to increase the wettability of the PANI/CDC ink on the graphite surface. Initially, a commercial graphite sheet current collector measuring 3 cm × 3 cm was affixed onto a PET film. The current collectors were coated with inks developed from pure CDC and PANI/CDC composites via the doctor blade method. The coated electrodes were dried for 1 h at 60 °C. Then, 0.5 M Na_2SO_4 electrolyte was dropped on the electrode until it was completely wet. The SCs were assembled by layering two identical electrodes and a cellulose separator paper (specifically, Dreamweaver Titanium AR40 cellulose paper). To seal the SCs, adhesive tape (specifically, 468 MP from 3 M) was utilized.

2.6. Fabrication of symmetrical SCs by screen printing

SCs were screen printed using PANI/CDC (10:1) and (30:1) variants. Samples were fabricated by screen printing a graphite current collector and a PANI/CDC electrode on two PET substrates, which constitute the positive and negative half of a SC. Screen printing was done using a sheet-to-sheet printing process, with a screen mesh count of 24 cm^{-1} and a thread diameter of 125 μm.

Current collectors were printed using a commercial graphite ink (Acheson ELECTRODAG PF-407C). After printing, the current collectors were dried at 95 °C for 1 h. Dried current collectors were treated with nitrogen plasma for 30 min to improve the wettability of the PANI/CDC ink on the graphite surface. Electrodes with geometrical area of 3 cm × 1 cm were then screen printed on top of the current collectors using the PANI/CDC ink, and afterwards dried at 60 °C for 30 min. The assembling was done in the same way as in the case of blade coated electrodes. The structure and real image of the fabricated SC was shown in figures 2(a) and (b).

2.7. Characterization methods

The Raman spectra, x-ray diffractograms (XRDs), x-ray photoelectron spectra (XPS), and Fourier transform infrared spectra were used to characterize the structure of PANI/CDC composites. The Raman spectra were recorded using the RAMAN Confocal Imaging System WITEC alpha300R with a 532 nm excitation laser. XRDs were obtained with a two-circle diffractometer XRD 3003 TT (GE Inspection Technology GmbH, Germany) with Cu-K radiation (k = 0.1542 nm). All XPS studies were carried out by means of an Axis Ultra photoelectron spectrometer (Kratos Analytical, Manchester, UK). The spectrometer was equipped with a monochromatic Al Kα ($h \times \nu$ = 1486.6 eV) x-ray source of 300 W at 15 kV.

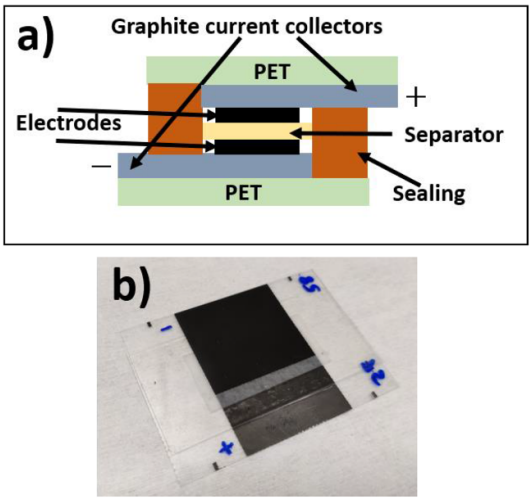

Figure 2. (a) Scheme of symmetrical two electrode supercapacitor, (b) photograph of an assembled supercapacitor.

The kinetic energy of photoelectrons was determined with hemispheric analyzer set to pass energy of 160 eV for wide-scan spectra and 20 eV for high-resolution spectra. Powdery samples were mounted as a thick particle film on the sample holder with double-sided adhesive tape (Scotch, 3 M Deutschland GmbH, Neuss, Germany). During all measurements, electrostatic charging of the sample was avoided by means of a low-energy electron source working in combination with a magnetic immersion lens. Later, all recorded peaks were shifted by the same value that was necessary to set the C 1 s peak to 285.00 eV. Quantitative elemental compositions were determined from peak areas using experimentally determined sensitivity factors and the spectrometer transmission function. Spectrum background was subtracted according to Shirley [44]. The high-resolution spectra were deconvoluted by means of the Kratos spectra deconvolution software. Free parameters of component peaks were their binding energy (BE), height, full width at half maximum and the Gaussian-Lorentzian ratio.

A scanning electron microscope (SEM, Carl Zeiss Microscopy Deutschland GmbH, Oberkochen, Germany) equipped with an XFlash 5060F energy-dispersive x-ray spectrometer (EDX) (Bruker Nano GmbH, Berlin, Germany) was utilized to characterize the morphologies of PANI, CDC, and PANI/CDC composites. Before analysis, the samples were coated with 3 nm Pt by sputter coating. Cross-section of PANI/CDC was prepared by embedding of composite in polystyrene film for EDX measurements. The cross-section block face was prepared with a diamond knife in an ultramicrotome, cutting the embedded particles. The SEM was operated at acceleration voltages of 3 kV and 6 kV for spectroscopy and 6 kV for element mapping. The thermal properties of the composite samples were examined by a thermogravimetric analyser [TGA Q5000 TA Instruments]. Thermal gravimetric analyses were carried out at a heating rate of 10 °C min^{-1} up to 800 °C after 10 min isothermal treatment at room temperature under a nitrogen atmosphere.

Using an in-house built device, the electrical powder conductivity of PANI, CDC, and PANI/CDC composites was evaluated. 50 mg of powder-like samples were tested in a poly (methyl methacrylate) (PMMA) cylinder with a 5 mm diameter cavity. The gold-plated plunger (also working as the upper electrode) presses the sample against the lower gold-plated electrode at defined pressures (5 MPa, 10 MPa, 20 MPa, 25 MPa, and 30 MPa) while simultaneously measuring pressure and electrode distance. According to the resistance detected by a multimeter (DMM 2001, Keithley Instruments, USA), the particle conductivity was calculated.

Standard cyclic voltammetry (CV) and galvanostatic charge-discharge (GCD) tests within established voltage ranges and at varying scan rates and current densities were used to evaluate the electrochemical characteristics of pure CDC and PANI/CDC composites. All electrochemical measurements were carried out using a conventional two-electrode and a three-electrode system on an Ivium-n-Stat potentiostat/galvanostat (Eindhoven, The Netherlands). The aqueous electrolyte utilized was 0.5 M Na_2SO_4. The counter electrode was a Pt coil and an Ag/AgCl was used as a reference electrode. In a three-electrode setup, the doctor-blade approach is used to prepare the working electrode. Graphite current collectors were first cut into 1 cm × 2 cm pieces. The collector is coated with the active material ink using a doctor blade (ERICHSEN MODEL 360, ERICHSEN GmbH & Co. KG, Germany) and a polyimide (Kapton®) film with a thickness of 50 μm as a mask. After drying, the electrode's active mass ranges from 1 to 5 mg.

The screen-printed SCs were characterized as per IEC 62391-1 standard, using a Maccor 4300 measuring device. A voltage window of 0.6 V was used for all measurements. Capacitance was calculated from 1 mA constant current discharge between 0.48 V and 0.24 V. ESR was calculated from the IR drop at the beginning of 10 mA constant current discharge. Leakage current was measured after holding the SC voltage at 0.6 V for 1 h. CV measurement was also performed to draw the cyclic voltammograms.

3. Results and discussions

Table 2 shows the electrical conductivity values of pristine PANI, CDC, and PANI/CDC powder composites measured at a pressure of 30 MPa. The highest conductivity of 23.6 S cm^{-1} was determined for the CDC powder. Pristine PANI has a conductivity of 0.09 S cm^{-1}. All composites possess a similar electrical conductivity compared to pristine PANI, which only slightly increases as the content of CDC

Table 2. Electrical conductivity of pure PANI and PANI/CDC powder composites at 30 MPa.

Sample	Powder conductivity (S/cm)
PANI	0.09
CDC	23.6
PANI/CDC (5:1)	0.4
PANI/CDC (10:1)	0.3
PANI/CDC (30:1)	0.1

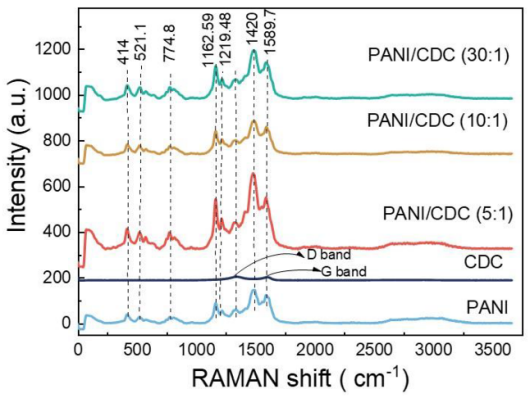

Figure 3. RAMAN spectra of pristine CDC, pristine PANI and PANI/CDC.

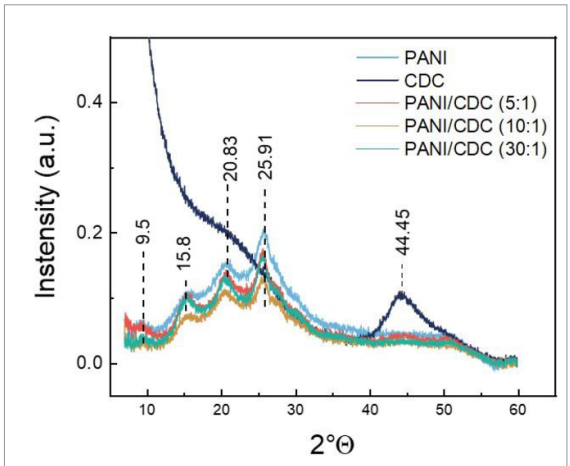

Figure 4. XRD patterns of pristine CDC, pristine PANI and PANI/CDC composites.

increases. The effect of the PANI conductivity on the composites is a hint for nearly complete coating of CDC by the *in-situ* grown PANI on the CDC surfaces. All composite materials are electrically conductive, a prerequisite for electron transfer in the final SC.

Figure 3 shows a summary of the Raman spectra for detection of structural characteristics of pristine CDC, PANI, and PANI/CDC composites. Two characteristic bands, the G-band at 1580–1600 cm^{-1} and the D-band at 1300–1350 cm^{-1}, have been identified in CDC spectra [45]. The Raman spectrum of the polyaniline salt shows the protonated emeraldine form, which is typical for as-prepared conductive PANI. All the characteristics of pure PANI can be found in the composites as well. Further descriptions of the specific bands of the RAMAN spectrum can be found in supplementary information (SI).

Figure 4 illustrates the XRD patterns of the specimens. Previous studies have shown that the peak at $2\theta = 44.45°$ (101) originates from graphite structure [46]. The diffraction pattern of pure PANI reveals broad peaks at $2\theta = 9.5°$, 15.8°, 20.83°, and 25.91°, which are characteristic of doped PANI [47, 48]. The composite also shows characteristic peaks of doped PANI that are absent in the XRD spectra of pure CDC, and these peaks are similar to those of the PANI/MWCNT composites we developed in our previous study [43]. When compared to the pristine PANI, the intensity of the diffraction peaks in the composites reduces with the inclusion of the CDC. This indicates that there may be a variation in degree of crystallinity between composites and pure PANI [49].

Figure 5 summarizes the XPS spectra, which were recorded from pristine PANI (a), pristine CDC (b) and the PANI/CDC composite (c). The N 1 s spectrum recorded from the pristine PANI is composed of the three component peaks *K*, *L*, and *M* resulting from photoelectrons escaped from the nitrogen atoms of PANI molecules in their electronic ground state. The most intense component peak *L* (at 399.26 eV) shows secondary amino groups that connect two phenyl rings (C–^{L}NH–C). As can be concluded from the presence of *shake-up* peaks in the N 1 s spectrum, electrons of the nitrogen atoms are involved in the highly conjugated π-electron system of PANI. Due to the polarization field caused by the easily mobile π-electrons the positive charge on the nitrogen atom can itself move away from its site. The corresponding structure observed in the PANI molecules is referred to as a polaron lattice. The source for the all other component peaks for pristine PANI were described in SI and our previous study [43].

The shape of the high-resolution C 1 s spectrum recorded from the pristine CDC (figure 5(b)) is dominated by a strongly asymmetric component peak *Gr* appearing at 284.08 eV. This is because the graphite-like lattice is composed of sp^2-hybridized carbon atoms, which were also identified in the pristine MWCNT in our prior study [43].

Figure 5(c) shows the high-resolution C 1 s and N 1 s XPS spectra recorded from the PANI/CDC (5-1). The composite formation of CDC and PANI did not lead to any significant changes in the high-resolution C 1 s and N 1 s XPS spectra recorded from the PANI/CDC (5-1), PANI/CDC (10-1), and PANI/CDC (30-1) samples. Since the BE values of the component peaks *Gr* (sp^2-hybridized carbon atoms of the graphene) and *Ph* (sp^2-hybridized carbon

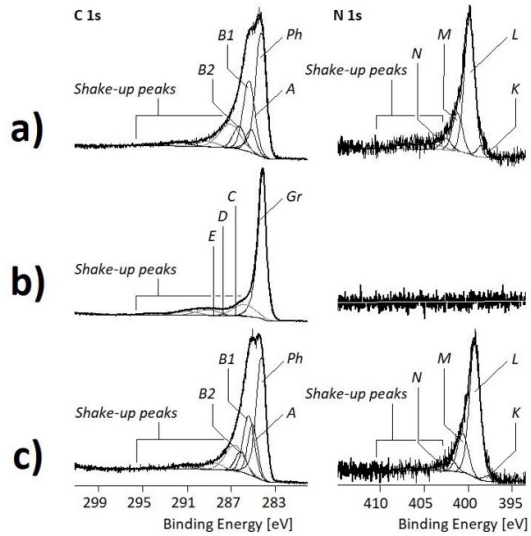

Figure 5. C 1 s (left column), and N 1 s (right column) high-resolution XPS spectra recorded from the pristine PANI polymer (a), pristine CDC (b), and PANI/CDC (5:1) composites (c).

Table 3. Relative nitrogen contents ([N]: [C]) of differently prepared PANI/CDC composite materials. The ratios were determined from normalized peak areas of the high-resolution C 1 s and N 1 s XPS.

	[N]: [C]
PANI	0.156
PANI/CDC (5:1)	0.153
PANI/CDC (10:1)	0.137
PANI/CDC (30:1)	0.151

atoms of the PANI polymer that do not have nitrogen atoms in their immediate vicinity) were about the same, no separations of the graphene fractions from the PANI fractions were possible in the C 1 s spectra. In previous research, we demonstrated that the PANI fractions on the surface of PANI/MWCNT composite materials could be estimated based on their relative nitrogen content ([N]: [C]) [43]. We employed the same characterization strategy in the current study to further understand the interaction between PANI and CDC.

As can be seen in table 3, even with an increasing PANI fraction, the relative nitrogen contents ([N]:[C]) of the PANI/CDC composite materials scatter around the value that was determined for the pristine polymer. This result indicates that the CDC particles are completely wrapped and coated by the PANI. Moreover, the conjugated π-electron system of PANI may cause good interaction through π–π stacking with the sp^2-hybridized carbons of the CDC in the final composite framework [50]. The detailed discussion of the XPS spectra is given in SI.

Figures 6(a)–(e) shows SEM images of pristine PANI, pristine CDC, and PANI/CDC composites with different aniline to carbon ratios. Pristine PANI (figure 6(b)) showed nanofibrillar and globular morphologies which are agglomerated. In the presence of PANI, a dramatic shift in the morphology of pristine CDC (figure 6(a)) was noticed. The SEM images of the PANI/CDC composites (figures 6(c)–(e)) indicate that the original agglomerate structure of CDC decomposes during composite preparation and PANI fully covers the CDC particles which also explains the dominating effect of PANI on the composite's conductivity. Both, granular structures and nanofibrillar morphology of the PANI/CDC composites increase the number of active sites of the electrode material. This will provide a larger surface area, and as a consequence will improve the overall performance of the SC, with respect to pristine CDC electrode (see below).

The SEM image, elemental maps, and EDX spectra of cross-sections of particles of the composite material embedded in polystyrene are displayed in figure 7. Both CDC and PANI, the two primary components of the composite, include C atoms. During the process of aniline polymerization, the oxidant APS and the reaction medium HCl are sources of S, O and Cl atoms. Si arises from contaminations. The expected elements of both PANI and CDC have been identified in the hybrid structure with S and Cl enriched at the surface of the particles, fitting to the coverage of CDC with PANI.

The thermal stability of pristine polyaniline, pristine CDC, and PANI/CDC composites was investigated and compared using TGA analysis. Figure 8 represent the TGA weight loss curves of pristine CDC, pristine PANI, and PANI/CDC composites, which were subjected to analysis under a nitrogen atmosphere. The pristine CDC is thermally stable with final weight loss at 800 °C of 3.4%. At ambient temperature, the pristine PANI and PANI/CDC composites undergo a weight loss of approximately 4 wt.% as a result of moisture loss within a 10 min isothermal treatment at the beginning of the measurement. Up to about 350 °C, the weight loss is caused by the further loss of water and other volatile substances. The most significant weight losses within the temperature range of 400 °C–650 °C, can be explained by the degradation of the polymeric backbone units, both, in the pristine PANI and PANI/CDC composites [51], exhibiting variations depending on the composite structure. The decomposition is finished at temperatures over 640 °C. Composite structures comply with similar weight loss steps, though with some variations. The TGA results indicate that the final weight loss of PANI/CDC (5:1), PANI/CDC (10:1), and PANI/CDC (30:1) increases with the PANI content, measuring at 47.5%, 51.3%, and 56%, respectively. The derivative weight loss curves and summary of thermal properties of pristine CDC, pristine PANI, and PANI/CDC composites are provided in figure S1 and table S1 in SI.

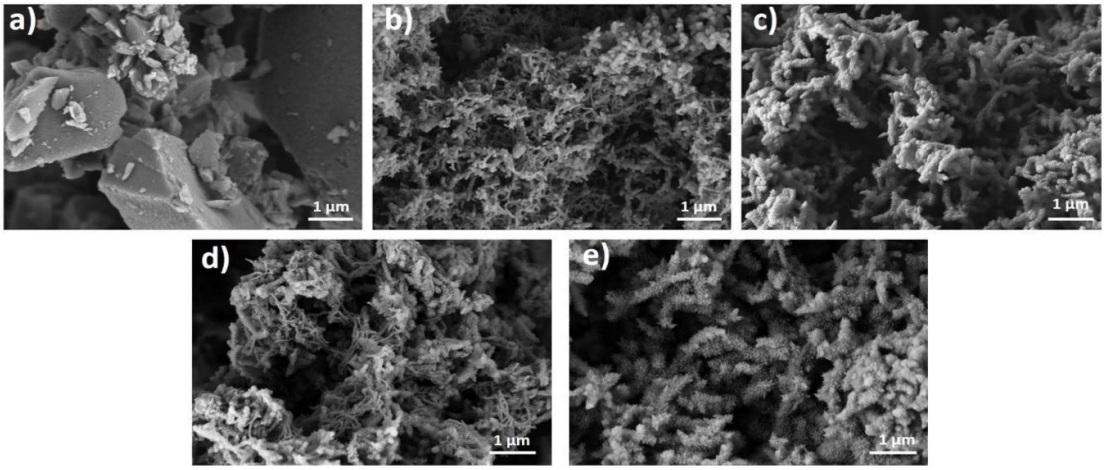

Figure 6. SEM images of (a) pristine CDC; (b) pristine PANI, (c) PANI/CDC- (5:1); (d) PANI/CDC- (10:1); (e) PANI/CDC- (30:1).

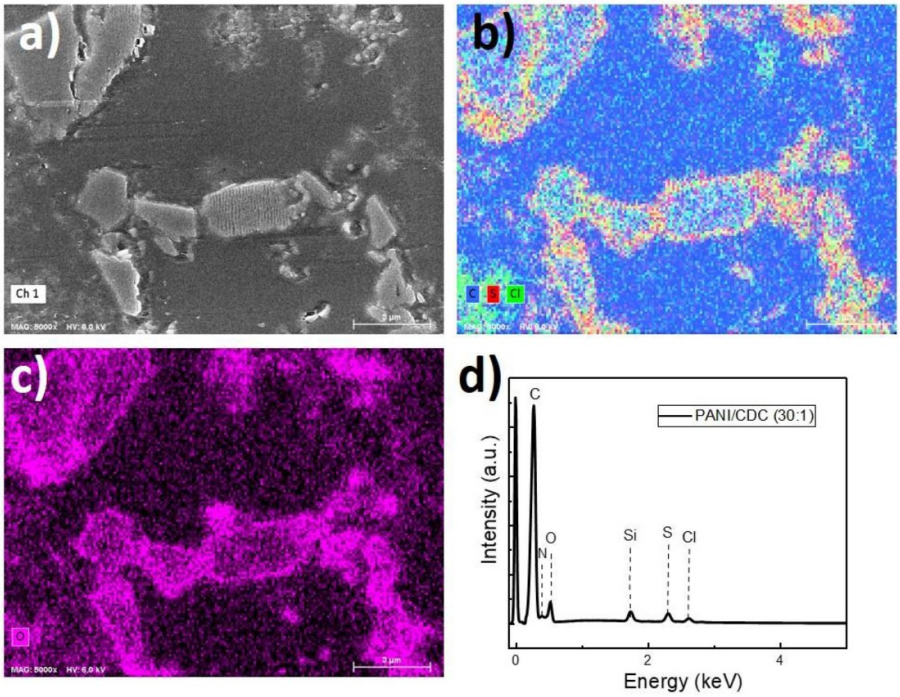

Figure 7. (a) SEM image and (b)–(c) elemental (C, S, Cl, O) mapping of cross sections of PANI/CDC (30:1) particles embedded in polystyrene. (d) EDX spectra of PANI/CDC (30:1) particles on silicon wafer (the yellow dots in (b) are superpositioned S and Cl atoms).

3.1. Results of electrochemical measurements

CV has been selected as the electrochemical measurement technique in order to investigate the material's overall electro-chemical behavior and to measure their specific capacitance. After electrode coating with chitosan binder via doctor blade method, the pristine PANI electrode exhibited a brittle behavior which hinders the realization of reliable electrochemical investigations. Therefore, the present study aimed to examine the comparison of pristine CDC and composites of PANI/CDC. Standard cyclic voltammograms of CDC and PANI/CDC composites were measured with a three-electrode system in the potential range from 0 V to 1 V using Ag/AgCl as a reference electrode. The specific capacitances (F g^{-1}) of samples were calculated from the CV plots according to the following equation,

$$C_{sp} = \frac{\int I(V)\,dV}{2m\Delta V\,v} \quad (1)$$

where $I(V)$ (A) represents the magnitude of current at a potential of V, ΔV represents the potential window, m (g) is the mass of active material in the WE, and v (V s^{-1}) is the potential scan rate.

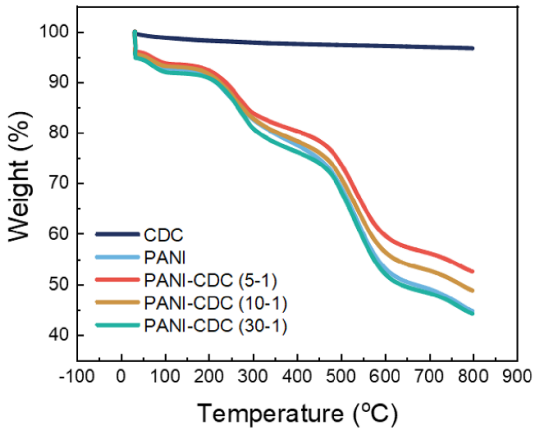

Figure 8. TGA weight loss curves of pristine PANI, pristine CDC and PANI/CDC composite.

Figure 9(a) compares the cyclic voltammograms of pure CDC and various PANI/CDC composites with 0.5 M Na_2SO_4 electrolyte at a scan rate of 50 mV s^{-1}. The pure CDC exhibits the typical rectangular form of an EDLCs, which demonstrates the presence of an electrostatic interaction between the electrode and the electrolyte. Lower electrochemical current is seen in the PANI/CDC (5:1) composite at a scan rate of 50 mV s^{-1}, which may lead to decreased electrochemical performance. In contrast to typical EDLCs behavior, the CV curves of the composites exhibit pseudocapacitance with Faradaic redox peaks between distinct PANI states [52]. Figure 9(b) shows the specific capacitance results of the composites at different scan rates. For composites, at all scan rates, the specific capacitance enhanced as the PANI content is increased. The PANI/CDC (30:1) composite demonstrated highest capacity across all samples for all scan rates. One reason may be the morphology of the composite, which exhibits elongated agglomerates of mostly fibril-like PANI particles (figure 6). Unfortunately, pure PANI electrode material could not be measured when using chitosan binder and Na_2SO_4 electrolyte due to the brittleness of the prepared film, demonstrating the importance of CDC as support in the composite. The composite PANI/CDC (5:1) has specific capacitance values of 281 F g^{-1}, 90 F g^{-1}, and 71 F g^{-1} at scan rates of 5 mV s^{-1}, 50 mV s^{-1}, and 100 mV s^{-1}, respectively. The specific capacitance values of PANI/CDC (10:1) are 344 F g^{-1}, 322 F g^{-1}, and 239 F g^{-1} at scan rates of 5 mV s^{-1}, 50 mV s^{-1} and 100 mV s^{-1}, respectively. The specific capacitance values of PANI/CDC (30:1) are 411 F g^{-1}, 246 F g^{-1}, and 232 F g^{-1} with the same scan rates, respectively. Table 4 shows a summary of these results. The cyclic voltammograms of pristine CDC and PANI/CDC electrodes with all scan rates are provided in figure S2 in SI.

The GCD test is the common method for evaluating the performance of SC materials. For this measurement, symmetric SCs were constructed using CDC and PANI/CDC electrodes and an aqueous electrolyte with 0.5 M Na_2SO_4. Figure 10(a) shows the GCD curves of the pristine CDC and PANI/CDC composites at a current density of 1 A g^{-1}. It is observed that the GCD curve of pristine CDC exhibits an ideal triangular shape, which is corroborated by the literature. The absence of ideal straight lines in the GCD curves of PANI/CDC SCs is consistent with previous studies and indicates the presence of a Faradaic reaction [53]. In accordance with the GCD curves of composite materials, a voltage drop may occur during the discharge process due mainly to internal resistances in the system [54, 55]. GCD curves of the PANI/CDC (30:1) composite are provided in the figure S3 in SI at different potential windows to investigate the relationship of the voltage drop with the applied potential. The results show that specific capacitance of SCs slightly increase with lower potential window (table S2).

Specific cell capacitances (C_{cell}, F g^{-1}) under different current densities (in A g^{-1}) were calculated with GCD measurements following the following equation:

$$C_{cell} = \frac{I \times \Delta t}{\Delta V \times M} \quad (2)$$

where I represent the magnitude of constant current during discharging, ΔV represents the potential window during discharging, Δt represent the discharging time and M represents the total active mass of electrodes. The specific capacitance of electrode material is:

$$C_{sp} = 4C_{cell}. \quad (3)$$

According to the GCD curves in figure 10(a), the specific capacitance values of pristine CDC, PANI/CDC (5:1), PANI/CDC (10:1), and PANI/CDC (30:1) are 144 F g^{-1}, 370 F g^{-1}, 398 F g^{-1}, and 419 F g^{-1} at current density of 1 A g^{-1}. The capacitance value of 144 F g^{-1} for pristine CDC relies within the range of other CDCs identified in previous studies, with variations in values possibly related to differences in carbide sources, electrolytes, and binders [56–58]. As a result, the specific capacitance value of the hybrid PANI/CDC composite is higher than that of pristine CDC. Considering the small quantity of research on PANI/CDC composites as an electrode material, it has to be emphasized that the acquired specific capacitance values are within the range reported in the existing literature [59].

There is currently no scientific research available on the use of chitosan binder and water-based inks within PANI/CDC composites electrodes. The energy density (E, W h kg^{-1}) values at various current

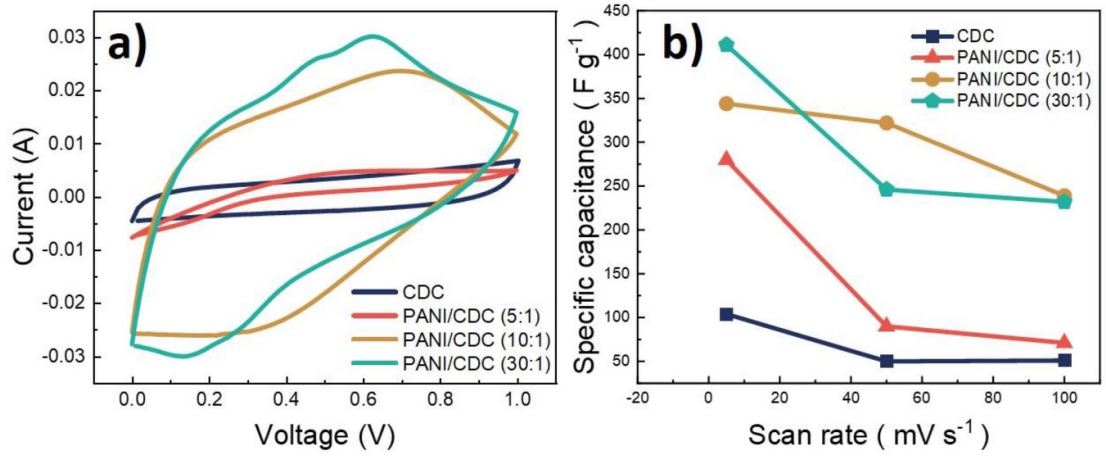

Figure 9. Cyclic voltammograms of PANI/CDC composites at a scan rate of 50 mV s $^{-1}$, and (b) specific capacitance values of pristine CDC and composites with different scan rates (5 mV s^{-1}, 50 mV s^{-1}, and 100 mV s^{-1}).

Table 4. Specific capacitance values of pristine CDC and composites with different scan rates, 5 mV s^{-1}, 50 mV s^{-1}, and 100 mV s^{-1}, respectively.

Sample	Specific capacitance at 5 mV s^{-1} (F g^{-1})	Specific capacitance at 50 mV s^{-1} (F g^{-1})	Specific capacitance at 100 mV s^{-1} (F g^{-1})
CDC	104	50	51
PANI/CDC (5:1)	281	90	71
PANI/CDC (10:1)	344	322	239
PANI/CDC (30:1)	411	246	232

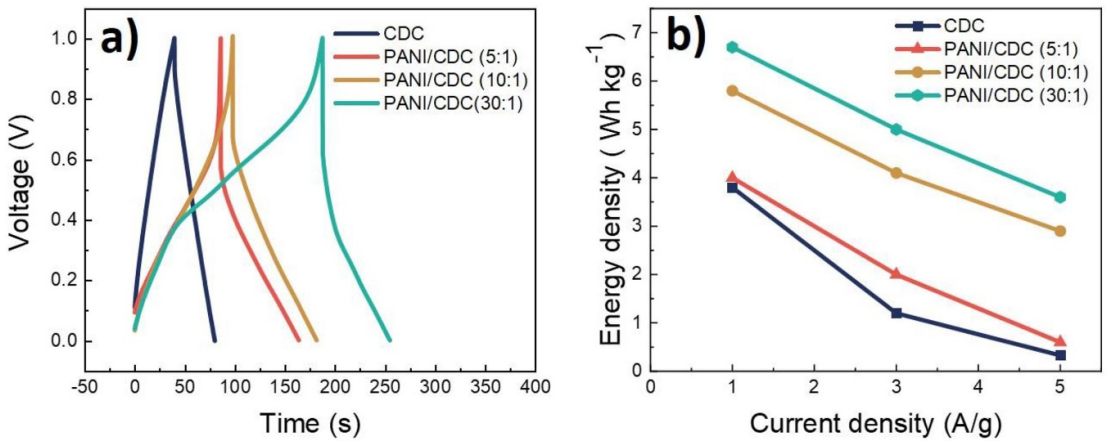

Figure 10. GCD curves of CDC, PANI/CDC (5:1), PANI/CDC (10:1), PANI/CDC (30:1) at 1 A g^{-1} and (b) specific capacitance values of pristine CDC and composites at different current densities (1 A g^{-1}, 3 A g^{-1}, and 5 A g^{-1}, respectively).

densities for pristine CDC and PANI/CDC SCs are shown in figure 10(b). The values are calculated based on GCD curves and calculated as:

$$E = \frac{C_{cell} \times (\Delta V)^2}{2 \times (3.6)} \quad (4)$$

where C_{cell} is cell capacitance (F g^{-1}) and ΔV is the potential window during the discharging after initial voltage drop. Table 5 summarizes the specific capacitance and energy density values, and power density values at 1 A g^{-1}. The composite PANI/CDC (5:1) has energy density values of 4 W h kg^{-1}, 2.1 W h kg^{-1}, and 0.6 W h kg^{-1} at current densities of 1 A g^{-1}, 3 A g^{-1}, and 5 A g^{-1}, respectively. The composite PANI/CDC (10:1) has energy density values of 5.8 W h kg^{-1}, 4.1 W h kg^{-1}, and 2.9 W h kg^{-1} at current densities of 1 A g^{-1}, 3 A g^{-1}, and 5 A g^{-1}, respectively. At the identical current densities, the composite PANI/CDC (30:1) has energy densities of 6.7 W h kg^{-1}, 5 W h kg^{-1}, and 3.6 W h kg^{-1}. According to the results, the highest energy density value of 6.7 W h kg^{-1} belongs to PANI/CDC (30:1) composites at 1 A g^{-1}, as expected. Pristine

Table 5. Specific capacitance, energy density, and power density values of CDC and PANI/CDC composites at current density of 1 A g^{-1}.

Sample	Specific capacitance (F g^{-1})	Energy density (W h kg^{-1})	Power density (W kg^{-1})
Pristine CDC	144	3.8	379.3
PANI/CDC (5:1)	370	4	186.6
PANI/CDC (10:1)	398	5.8	262.1
PANI/CDC (30:1)	419	6.7	367.5

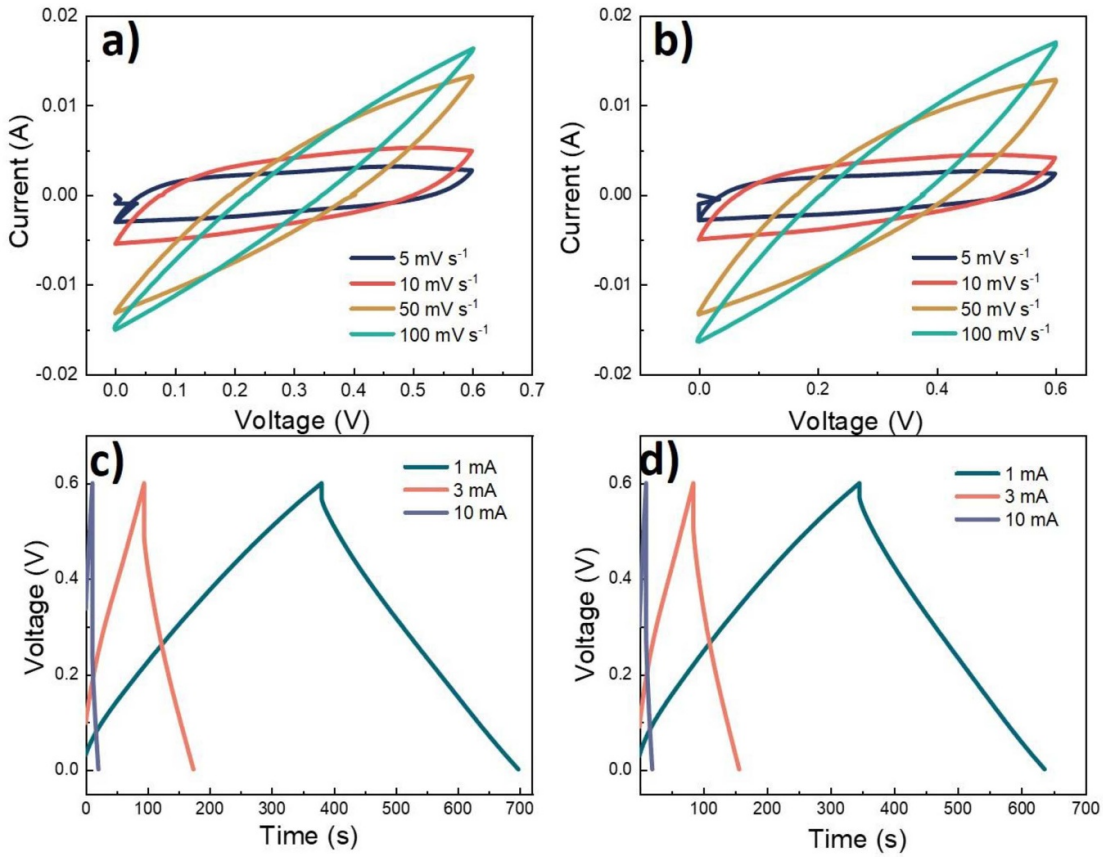

Figure 11. Cyclic voltammograms of a typical screen printed symmetric PANI/CDC (10:1) supercapacitor (a) and PANI/CDC (30:1) supercapacitor (b) at different scan rates (5 mV s^{-1}, 10 mV s^{-1}, 50 mV s^{-1}, and 100 mV s^{-1}); GCD curves of a typical screen printed PANI/CDC (10:1) supercapacitor (c) and a PANI/CDC (30:1) supercapacitor (d) at different current levels (1 mA, 3 mA, 10 mA).

CDC has the lowest energy density value which is 0.3 W h kg^{-1} at 5 A g^{-1}. The energy density values increase when the aniline/carbon weight ratio increases. Furthermore, the PANI/CDC (30:1) composites possessed the highest power density of all composites of 367.5 W kg^{-1} at 1 A g^{-1}, which is comparable to pristine CDC. The power density values are calculated based on GCD curves and calculated as:

$$P = \frac{E \times 3600}{\Delta t}$$

where E is the energy density (Wh kg^{-1}) and Δt is the discharge time.

3.2. Electrochemical measurements of screen-printed SCs

PANI/CDC (10:1) and PANI/CDC (30:1) were selected as composite inks for screen printing, and inks were formulated with an eco-friendly chitosan binder in water-based media. The fabricated ink layers were successfully screen printed on top of the current collector. The nitrogen plasma treatment was found to be essential for screen printing process to increase wettability of a surface of the current collector. Without surface treatment most of the ink did not transfer from the screen to top of the current collector. PANI/CDC ink showed shear thinning behavior, with viscosity ranging between 100 and 1000 Pa s, which makes it suitable for screen printing operations. The CV and galvanostatic measurements to define the electrical properties of screen-printed SCs are presented in figures 11(a)–(d).

Table 6 presents the mean and standard deviation of measured capacitance, ESR and leakage current values of the screen-printed SCs. An unequal variances t-test was used to test, whether the mean

Table 6. Mean and standard deviation of capacitance, ESR and leakage current measured from screen printed samples; p-values for testing equality of means between (10:1) and (30:1).

	Capacitance (mF)		ESR (Ω)		Leakage current (mA)	
	Mean	Std. Dev	Mean	Std. Dev	Mean	Std. Dev
PANI/CDC (10:1) $N = 10$	469.5	59.5	27.0	6.2	427.5	67.8
PANI/CDC (30:1) $N = 10$	443.8	43.4	27.2	2.0	409.4	48.8
p-value	0.286		0.921		0.504	

values between the (10:1) and (30:1) variants are equal. Using a significance level of 0.05 for each test, it is concluded that no statistically significant difference in capacitance, ESR or leakage current is observed between screen printed PANI/CDC (10:1) and PANI/CDC (30:1) SCs. It can be concluded that the screen-printing process is a feasible and repeatable way to fabricate SCs with PANI/CDC electrodes.

4. Conclusion

In this study, PANI/CDC hybrid composites were synthesized by *in-situ* chemical oxidative polymerization of aniline in presence of CDC. The morphology of the PANI/CDC composites show that PANI particles were successfully coated to the carbon surface. Therefore, the electrical conductivity of the composites powder is dominated by the conductivity of PANI. Printable PANI/CDC ink materials were developed based on chitosan binder in water media and with 0.5 M Na_2SO_4 as electrolyte, while pure PANI ink without CDC was not printable because of its fragile structure. The symmetrical SCs of PANI/CDC composites were successfully fabricated by using both, doctor blade coating and screen printing.

Electrochemical measurements were done with both, three electrode and two electrode measurements. As a result of the combination of electrostatic charge accumulation and reversible redox processes at the interface between electrode and electrolyte, the PANI/CDC composites provided a significant higher specific capacitance (up to 419 F g^{-1} at 1 Ag^{-1}) than the pristine CDC electrode (144 F g^{-1} at 1 A g^{-1}). The capacitance of screen-printed SCs was 440–470 mF with an ESR of about 27 Ω. This research indicates that it is feasible to implement a screen-printing approach for manufacturing electrodes using carbon-based polymer composite inks by using non-toxic chitosan binder. Such results may pave the way for future sustainable and commercial energy storage applications of screen-printable SCs.

Data availability statement

All data that support the findings of this study are included within the article (and any supplementary files).

Acknowledgments

We appreciate Christine Steinbach for the BET test, Dieter Fischer and Julia Muche for the Raman test, Manuela Heber for SEM analysis, Petr Formanek for EDX and TEM analysis, Regine Boldt for XRD analysis, Kerstin Arnold for TGA analysis and the Skeleton Technologies for providing the CDC (trade mark name-Curved Graphene).

This work has received funding from the European Union's Horizon 2020 Research and Innovation Programme for project InComEss under Grant Agreement Number 862597.

Screen printing investigation uses Academy of Finland Research Infrastructure 'Printed Intelligence Infrastructure' (PII-FIRI, Grant No. 320019).

Author contributions

The manuscript was written through contributions of all authors. All authors have given approval to the final version of the manuscript.

E I Y: Data curation, Formal Analysis, Investigation, Methodology, Validation, Visualization, Writing—original draft; J P: Conceptualization, Funding acquisition, Methodology, Project administration, Supervision, Writing—review & editing; J K: Conceptualization, Resources, Supervision, Validation, Writing—review & editing; A K: Data curation, Formal analysis, Investigation, Writing—original draft; T P: Investigation, Writing—review & editing; F S: Data curation, Formal Analysis, Validation, review & editing; M M: Conceptualization, Funding acquisition, Methodology, Project administration, Supervision, Writing—review & editing; B V: Data curation, Resources, Supervision, Writing—review & editing.

ORCID iDs

Ezgi Inci Yesilyurt https://orcid.org/0000-0001-9657-3812
Jürgen Pionteck https://orcid.org/0000-0003-2310-1106
Jari Keskinen https://orcid.org/0000-0002-3144-972X
Frank Simon https://orcid.org/0000-0002-4063-1742

Matti Mäntysalo https://orcid.org/0000-0002-7780-6454
Brigitte Voit https://orcid.org/0000-0002-4531-691X

References

[1] Zhang S and Pan N 2015 Supercapacitors performance evaluation *Adv. Energy Mater.* **5** 1401401
[2] González A, Goikolea E, Barrena J A and Mysyk R 2016 Review on supercapacitors: technologies and materials *Renew. Sustain. Energy Rev.* **58** 1189–206
[3] Zhang L L and Zhao X 2009 Carbon-based materials as supercapacitor electrodes *Chem. Soc. Rev.* **38** 2520–31
[4] Lu M 2013 *Supercapacitors: Materials, Systems, and Applications* (Wiley) (https://doi.org/10.1002/9783527646661)
[5] Wu N, Bai X, Pan D, Dong B, Wei R, Naik N, Patil R R and Guo Z 2021 Recent advances of asymmetric supercapacitors *Adv. Mater. Interfaces* **8** 2001710
[6] Vangari M, Pryor T and Jiang L 2013 Supercapacitors: review of materials and fabrication methods *J. Energy Eng.* **139** 72–79
[7] Bryan A M, Santino L M, Lu Y, Acharya S and D'Arcy J M 2016 Conducting polymers for pseudocapacitive energy storage *Chem. Mater.* **28** 5989–98
[8] Chen W, Xia C, Rakhi R B and Alshareef H N 2014 A general approach toward enhancement of pseudocapacitive performance of conducting polymers by redox-active electrolytes *J. Power Sources* **267** 521–6
[9] Wang H, Liu J, Chen Z, Chen S, Sum T C, Lin J and Shen Z X 2017 Synergistic capacitive behavior between polyaniline and carbon black *Electrochim. Acta* **230** 236–44
[10] Eftekhari A, Li L and Yang Y 2017 Polyaniline supercapacitors *J. Power Sources* **347** 86–107
[11] Wang H, Lin J and Shen Z X 2016 Polyaniline (PANi) based electrode materials for energy storage and conversion *J. Sci. Adv. Mater. Dev.* **1** 225–55
[12] Yu H, Xin G, Ge X, Bulin C, Li R, Xing R and Zhang B 2018 Porous graphene-polyaniline nanoarrays composite with enhanced interface bonding and electrochemical performance *Compos. Sci. Technol.* **154** 76–84
[13] Branzoi V, Branzoi F and Pilan L 2010 Electrochemical fabrication and capacitance of composite films of carbon nanotubes and polyaniline *Surf. Interface Anal.* **42** 1266–70
[14] Lin H, Li L, Ren J, Cai Z, Qiu L, Yang Z and Peng H 2013 Conducting polymer composite film incorporated with aligned carbon nanotubes for transparent, flexible and efficient supercapacitor *Sci. Rep.* **3** 1353
[15] Zhao X, Gnanaseelan M, Jehnichen D, Simon F and Pionteck J 2019 Green and facile synthesis of polyaniline/tannic acid/rGO composites for supercapacitor purpose *J. Mater. Sci.* **54** 10809–24
[16] Abioye A M and Ani F N 2015 Recent development in the production of activated carbon electrodes from agricultural waste biomass for supercapacitors: a review *Renew. Sustain. Energy Rev.* **52** 1282–93
[17] Faraji S and Ani F N 2015 The development supercapacitor from activated carbon by electroless plating—A review *Renew. Sustain. Energy Rev.* **42** 823–34
[18] Pekala R, Farmer J C, Alviso C T, Tran T D, Mayer S T, Miller J M and Dunn B 1998 Carbon aerogels for electrochemical applications *J. Non-Cryst. Solids* **225** 74–80
[19] Han Y, Ha H, Choi C, Yoon H, Matteini P, Cheong J Y and Hwang B 2023 Review of flexible supercapacitors using carbon nanotube-based electrodes *Appl. Sci.* **13** 3290
[20] Ke Q and Wang J 2016 Graphene-based materials for supercapacitor electrodes–A review *J. Materiom.* **2** 37–54
[21] Torop J, Palmre V, Arulepp M, Sugino T, Asaka K and Aabloo A 2011 Flexible supercapacitor-like actuator with carbide-derived carbon electrodes *Carbon* **49** 3113–9
[22] Yushin G, Nikitin A and Gogotsi Y 2006 *Carbide Derived Carbon* (Carbon Nanomater) pp 211–54
[23] Gu W and Yushin G 2014 Review of nanostructured carbon materials for electrochemical capacitor applications: advantages and limitations of activated carbon, carbide-derived carbon, zeolite-templated carbon, carbon aerogels, carbon nanotubes, onion-like carbon, and graphene *Wiley Int. Rev. Energy Environ.* **3** 424–73
[24] Rajeevan S, John S and George S C 2021 Polyvinylidene fluoride: a multifunctional polymer in supercapacitor applications *J. Power Sources* **504** 230037
[25] Park H-K, Kong B-S and Oh E-S 2011 Effect of high adhesive polyvinyl alcohol binder on the anodes of lithium ion batteries *Electrochem. Commun.* **13** 1051–3
[26] Aslan M, Weingarth D, Jäckel N, Atchison J S, Grobelsek I and Presser V 2014 Polyvinylpyrrolidone as binder for castable supercapacitor electrodes with high electrochemical performance in organic electrolytes *J. Power Sources* **266** 374–83
[27] Cheng S, Liu H and Logan B E 2006 Power densities using different cathode catalysts (Pt and CoTMPP) and polymer binders (Nafion and PTFE) in single chamber microbial fuel cells *Environ. Sci. Technol.* **40** 364–9
[28] Karkar Z, Guyomard D, Roué L and Lestriez B 2017 A comparative study of polyacrylic acid (PAA) and carboxymethyl cellulose (CMC) binders for Si-based electrodes *Electrochim. Acta* **258** 453–66
[29] Zhu Z, Tang S, Yuan J, Qin X, Deng Y, Qu R and Haarberg G M 2016 Effects of various binders on supercapacitor performances *Int. J. Electrochem. Sci.* **11** 8270–9
[30] Bresser D, Buchholz D, Moretti A, Varzi A and Passerini S 2018 Alternative binders for sustainable electrochemical energy storage–the transition to aqueous electrode processing and bio-derived polymers *Energy Environ. Sci.* **11** 3096–127
[31] Salleh N A, Kheawhom S and Mohamad A A 2021 Chitosan as biopolymer binder for graphene in supercapacitor electrode *Results Phys.* **25** 104244
[32] Yang X, Tu Y, Li L, Shang S and Tao X-M 2010 Well-dispersed chitosan/graphene oxide nanocomposites *ACS Appl. Mater. Interfaces* **2** 1707–13
[33] Keskinen J, Railanmaa A and Lupo D 2018 Monolithically prepared aqueous supercapacitors *J. Energy Storage* **16** 243–9
[34] Salleh N A, Kheawhom S, Ashrina A Hamid N, Rahiman W and Mohamad A A 2023 Electrode polymer binders for supercapacitor applications: a review *J. Mater. Res. Technol.* **23** 3470–91
[35] Yang H, Ji X, Tan Y, Liu Y and Ran F 2019 Modified supramolecular carboxylated chitosan as hydrogel electrolyte for quasi-solid-state supercapacitors *J. Power Sources* **441** 227174
[36] Zhong C *et al* 2015 A review of electrolyte materials and compositions for electrochemical supercapacitors *Chem. Soc. Rev.* **44** 7484–539
[37] Hosseini M G, Shahryari E and Yardani Sefidi P 2021 Polyaniline grafted chitosan/GO-CNT/Fe3O4 nanocomposite as a superior electrode material for supercapacitor application *J. Appl. Polym. Sci.* **138** 50976
[38] Padwal P, Kadam S L, Mane S M and Kulkarni S B 2016 Synthesis and characterization of supercapacitive behavior of electrodeposited PANI/Co3O4 layered composite electrode *J. Chin. Adv. Mater. Soc.* **4** 13–23
[39] Li H and Liang J 2020 Recent development of printed micro-supercapacitors: printable materials, printing technologies, and perspectives *Adv. Mater.* **32** 1805864
[40] Gao Y, Guo X, Qiu Z, Zhang G, Zhu R, Zhang Y and Pang H 2022 Printable electrode materials for supercapacitors *ChemPhysMater* **1** 17–38
[41] Zheng L, Wang Y, Wang X, Li N, An H, Chen H and Guo J 2010 The preparation and performance of calcium carbide-derived carbon/polyaniline composite electrode material for supercapacitors *J. Power Sources* **195** 1747–52

[42] Tang S-J, Wang A-T, Lin S-Y, Huang K-Y, Yang C-C, Yeh J-M and Chiu K-C 2011 Polymerization of aniline under various concentrations of APS and HCl *Polym. J.* **43** 667–75
[43] Inci Yesilyurt E, Pionteck J, Simon F and Voit B 2023 Fabrication of PANI/MWCNT supercapacitors based on a chitosan binder and aqueous electrolyte for enhanced energy storage *RSC Appl. Polym.* **1** 97–110
[44] Shirley D A 1972 High-resolution x-ray photoemission spectrum of the valence bands of gold *Phys. Rev.* B **5** 4709
[45] Urbonaite S, Hälldahl L and Svensson G 2008 Raman spectroscopy studies of carbide derived carbons *Carbon* **46** 1942–7
[46] Gaidukevic J, Aukstakojyte R, Navickas T, Pauliukaite R and Barkauskas J 2021 A novel approach to prepare highly oxidized graphene oxide: structural and electrochemical investigations *Appl. Surf. Sci.* **567** 150883
[47] Singu B S, Srinivasan P and Pabba S 2011 Benzoyl peroxide oxidation route to nano form polyaniline salt containing dual dopants for pseudocapacitor *J. Electrochem. Soc.* **159** A6
[48] Abdiryim T, Jamal R and Nurulla I 2007 Doping effect of organic sulphonic acids on the solid-state synthesized polyaniline *J. Appl. Polym. Sci.* **105** 576–84
[49] Terohid S, Heidari S, Jafari A and Asgary S 2018 Effect of growth time on structural, morphological and electrical properties of tungsten oxide nanowire *Appl. Phys.* A **124** 1–9
[50] Sreevidya U, Shalini V, Kavirajan S, Maiyelvaganan K R, Prakash M, Kamala Bharathi K, Senthil Kumar E, Archana J, Harish S and Navaneethan M 2023 Investigation of non-covalent interactions in polypyrrole/polyaniline/carbon black ternary complex for enhanced thermoelectric properties via interfacial carrier scattering and π-π stacking *J. Colloid Interface Sci.* **630** 46–60
[51] Kumar A *et al* 2020 Synthesis and thermal analysis of polyaniline (PANI) *J. Phys.: Conf. Ser.* **1531** 012108
[52] Kang E, Neoh K and Tan K 1998 Polyaniline: a polymer with many interesting intrinsic redox states *Prog. Polym. Sci.* **23** 277–324
[53] Jiang Y and Liu J 2019 Definitions of pseudocapacitive materials: a brief review *Energy Environ. Mater.* **2** 30–37
[54] An K H, Kim W S, Park Y S, Choi Y C, Lee S M, Chung D C, Bae D J, Lim S C and Lee Y H 2001 Supercapacitors using single-walled carbon nanotube electrodes *Adv. Mater.* **13** 497–500
[55] Prasad G G *et al* 2019 Supercapacitor technology and its applications: a review *IOP Conf. Ser. Mater. Sci. Eng.* **561** 012105
[56] Thomberg T, Jänes A and Lust E 2010 Energy and power performance of electrochemical double-layer capacitors based on molybdenum carbide derived carbon *Electrochim. Acta* **55** 3138–43
[57] Fernandez J, Arulepp M, Leis J, Stoeckli F and Centeno T A 2008 EDLC performance of carbide-derived carbons in aprotic and acidic electrolytes *Electrochim. Acta* **53** 7111–6
[58] Chmiola J, Yushin G, Dash R and Gogotsi Y 2006 Effect of pore size and surface area of carbide derived carbons on specific capacitance *J. Power Sources* **158** 765–72
[59] Yang J *et al* 2023 Modification and supercapacitive performance enhancement of calcium carbide-derived carbon prepared by a green solvent-free mechanochemical route *ACS Appl. Energy Mater.* **6** 6029–40